METHOD OF MOMENTS ANALYSIS OF SLOTTED WAVEGUIDE ANTENNA ARRAYS

A THESIS SUBMITTED TO
THE GRADUATE SCHOOL OF NATURAL AND APPLIED SCIENCES
OF
MIDDLE EAST TECHNICAL UNIVERSITY

BY

ABDÜLKERİM ALTUNTAŞ

IN PARTIAL FULFILLMENT OF THE REQUIREMENTS
FOR
THE DEGREE OF MASTER OF SCIENCE
IN
ELECTRICAL AND ELECTRONICS ENGINEERING

FEBRUARY 2014

Approval of the Thesis:

METHOD OF MOMENTS ANALYSIS OF SLOTTED WAVEGUIDE ANTENNA ARRAYS

submitted by **ABDÜLKERİM ALTUNTAŞ** in partial fulfillment of the requirements for the degree of **Master of Science in Electrical and Electronics Engineering Department, Middle East Technical University** by,

Prof. Dr. Canan ÖZGEN
Dean, Graduate School of **Natural and Applied Sciences** _____

Prof. Dr. Gönül TURHAN SAYAN
Head of Department, **Electrical and Electronics Engineering** _____

Assoc. Prof. Dr. Lale ALATAN
Supervisor, **Electrical and Electronics Engineering Dept., METU** _____

Examining Committee Members:

Prof. Dr. Gülbin DURAL
Electrical and Electronics Engineering Dept., METU _____

Assoc. Prof. Dr. Lale ALATAN
Electrical and Electronics Engineering Dept., METU _____

Prof. Dr. Özlem AYDIN ÇİVİ
Electrical and Electronics Engineering Dept., METU _____

Assis. Prof. Dr. Özgür ERGÜL
Electrical and Electronics Engineering Dept., METU _____

Can Barış TOP (Ph.D.)
ASELSAN A.Ş. _____

Date: 07.02.2014

I hereby declare that all information in this document has been obtained and presented in accordance with academic rules and ethical conduct. I also declare that, as required by these rules and conduct, I have fully cited and referenced all material and results that are not original to this work.

Name, Last name: Abdülkerim ALTUNTAŞ

Signature :

ABSTRACT

METHOD OF MOMENTS ANALYSIS OF SLOTTED WAVEGUIDE ANTENNA ARRAYS

ALTUNTAŞ, Abdülkerim

M.S., Department of Electrical and Electronics Engineering
Supervisor: Assoc. Prof. Dr. Lale ALATAN

February 2014, 54 pages

Slotted waveguide antenna arrays are used extensively in many applications because of their high power handling capability, planarity, low loss and reduced profile. After the synthesis of such an array, the design should be verified by analyzing the array with an efficient simulation tool which is accurate, fast and flexible. Although FEM (Finite Element Method) based commercial softwares are very accurate and flexible, they are not sufficiently fast especially when it comes to optimization and fine tuning. The aim of this study is to develop a MoM based simulation software to analyze slotted waveguide antenna arrays. The developed code is aimed to be a building block for a versatile software capable of analyzing different structures, so the code is designed to be open for future manipulations and improvements. A single slot on a waveguide is analyzed by using the developed code and the self admittance of the slot is calculated for different slot offset and length values. The results are compared with the experimental results found in the literature and a fair agreement is observed.

Keywords: Slotted Waveguide Antenna Arrays, Method of Moments

ÖZ

YARIKLI DALGA KILAVUZU DİZİ ANTENLERİNİN MOMENTLER YÖNTEMİYLE ANALİZİ

ALTUNTAŞ, Abdülkerim

Yüksek Lisans, Elektrik ve Elektronik Mühendisliği Bölümü
Tez Yöneticisi: Doç. Dr. Lale ALATAN

Şubat 2014, 54 sayfa

Yarıklı dalga kılavuzu anten dizileri yüksek güce dayanıklılığı, düzlemselliği, düşük araya girme kaybı ve küçük kesitleri gibi özelliklerinden ötürü sıklıkla birçok alanda kullanılmaktadır. Diziyi sentezledikten sonra, tasarım hassas, hızlı ve esnek bir benzetim programıyla incelenerek doğrulanmalıdır. FEM (Sonlu Eleman Yöntemi) temelli ticari benzetim programları oldukça hassas ve esnek olmalarına rağmen optimizasyon ve ince ayar yapmak için yeteri kadar hızlı değillerdir. Bu çalışmanın amacı yarıklı dalga kılavuzu anten dizilerini analiz eden MoM temelli bir benzetim yazılımı geliştirmektir. Geliştirilen kodun farklı yapıları analiz edebilen geniş kapsamlı bir yazılımın temel taşlarından biri olması hedeflendiği için yazılım ileriye yönelik kullanımlara ve geliştirmelere açık olacak şekilde tasarlanmıştır. Dalga kılavuzu üzerindeki tek bir yarık geliştirilen yazılım kullanılarak analiz edilmiş ve yarığın özadmitansı farklı merkeze uzaklık ve uzunluk değerleri için hesaplanmıştır. Sonuçlar literatürde bulunan ölçüm değerleri ile karşılaştırılmış ve makul bir uyum gözlenmiştir.

Anahtar Kelimeler: Yarıklı Dalga Kılavuzu Dizisi Antenler, Momentler Yöntemi

To My Family

ACKNOWLEDGMENTS

The author would like to express his sincere appreciation to his supervisor, Assoc. Prof. Dr. Lale ALATAN for her valuable guidance and supervision. Without her support this work would not be possible.

The author would like to acknowledge his gratitude to his friends and colleagues in ASELSAN A.Ş.. A special thanks goes to Can Barış TOP who supported the author with his experience about the topic.

Last but not the least, the author would like to express his deepest gratitude to his parents, without whom he would never have been able to reach where he is.

TABLE OF CONTENTS

LIST OF FIGURES

FIGURES

LIST OF TABLES

TABLES

CHAPTER 1

INTRODUCTION

Slotted waveguide antenna arrays are widely used in applications requiring high power handling capability, low insertion loss, planarity and low profile specifications such as radars, satellites and remote sensing. These antennas are basically formed by cutting narrow slots on the broad or narrow walls of the waveguide which are placed periodically. There are several radiating slot elements such as longitudinal, transversal or inclined slots cut on the broad wall of the waveguide as well as inclined I or C shaped slots cut on the narrow wall [1] as shown in Figure 1-1. There are two types of these antennas, namely travelling wave and standing wave antennas. In travelling wave antennas the end of the array is terminated with a matched load, whereas in the standing wave type the termination is a short circuit. In this work the focus is given on travelling wave arrays with longitudinal slots cut on the broad wall of the waveguide.

The basic property of these slots is that they become resonant at nearly a half wavelength long and their radiation characteristics can be controlled by their mechanical parameters namely, the slot offset from the center line of the waveguide and the length. Such a controlling mechanism makes one able to design an array of specific center frequency, side lobe level, beam width and return loss.

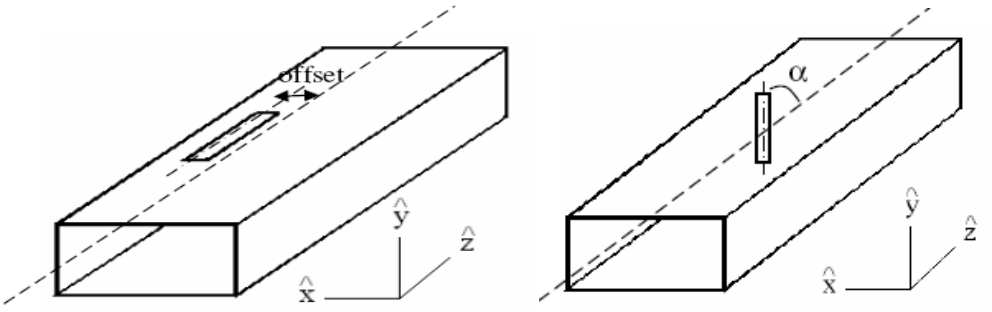

(a) Longitudinal slot on the broad wall (b) Inclined slot on the broad wall

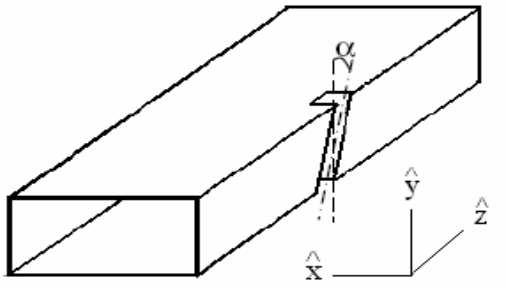

(c) Inclined slot on the narrow wall

Figure 1-1 Numerous types of radiating slots in a waveguide

Slotted waveguide structures are being extensively used since late 1940's. Watson, Stevenson and Booker conducted the first works about this topic. Stevenson brought theoretical meaning to Watson's experimental work by formulating the electric field of the slot aperture. Booker was the one who solved the integral equation making use of the waveguide Green's functions and the analogy between dipoles and slots based on Babinet's principle [2]-[4]. Stegen conducted an experimental work on the admittance and resonant length of a longitudinal broad wall slot with respect to its offset. He was able to generate universal curves for the admittance of a slot as a

function of its length normalized to its resonant length [5]. This process is called the characterization of a single slot and must be carried out either experimentally or numerically before the design of a linear slotted waveguide array. Once this process has been gone through, characterization data of the single slot is gathered which is to be used in the design procedure.

In 1979, Elliott published a paper in which he explains the design steps of a slotted waveguide array of travelling type [6]. This design procedure to synthesize such an array of slots is as follows:

a) According to the frequency of operation and application dependent size, determine the waveguide to be used. For example, in an X-Band radar application, standard WR90 waveguide might be used; however, if there is some sort of limitation in the dimensions, one might also think of using ridged waveguide to reduce the dimensions.
b) Either by experiments or by full wave simulation tools like the Finite Element Method based HFSS by Ansoft, perform the characterization of a single isolated slot. Characterization of a single slot corresponds to obtaining the admittance of this slot for several offset and length values. Generally 6-7 different slot offset and 6-7 different slot length values are sufficient. Then slot admittance values for other offset and length values can be interpolated [1].
c) From these admittance values, the following four characterization polynomials are extracted:
   - ⇨ $g(x)$: Resonant conductance as a function of slot offset, x.
   - ⇨ $v(x)$: Resonant length as a function of slot offset, x.
   - ⇨ $h_1(y)$: Conductance of the slot normalized with respect to the resonant conductance. y is the slot length normalized with respect to the resonant length corresponding to the specified offset.

⇨ $h_2(y)$: Susceptance of the slot normalized with respect to the resonant conductance. y is the slot length normalized with respect to the resonant length corresponding to the specified offset.

Resonant length is the length of the slot for which the imaginary part of the slot admittance is zero. The slot conductance corresponding to this length is called the resonant conductance.

These four polynomials model the isolated slot admittance as a function of the slot offset and length. They are used in the design equations derived by Elliott [6].

d) According to the required side lobe level, beam width, main beam direction, directivity and input matching level, determine the number of elements to be used in the array, the inter element spacing of the array and the excitation coefficient of each slot (i.e. slot voltage).

e) Make an initial guess for the slot lengths and offsets and compute the mutual coupling term for each slot.

f) Since the design is a travelling wave type array, it is going to be terminated by a matched load. Make an initial guess on the slot offset for the last element, the element just before the matched load, since the whole array will be designed iteratively according to the last element. Furthermore, this offset is also important for the delivered power to the load. Practically, the array is designed such that 5-10% of the input power is delivered to the load.

g) Using the design equations and beginning from the last slot, adjust the offset and length of every element such that it becomes resonant at the center frequency and satisfies the required slot voltage.

h) With the new slot offset and length values compute the mutual coupling term for each element.

i) Repeat step g and h until all new offset and lengths of the elements converge, i.e. the newly found offset and length values are negligibly different than the previous ones.

j) At that point, check the followings:

- ⇨ Input match: If the match is not good enough, change the distance between the slots.
- ⇨ Maximum slot offset in the array: If this slot offset is very large, the design equations based on the equivalent circuit that models the slot with a shunt admittance, becomes invalid. Hence, repeat the above procedure with a smaller offset for the last slot.
- ⇨ Power delivered to the termination: If the power absorbed by the load does not meet the design criterion, alter the offset of the last slot.

After the synthesis is accomplished, the next step is to validate the design, i.e. to analyze it and check that the design criteria are satisfied. This is generally done using advanced simulation tools such as Ansoft HFSS [7] and WASP-NET [8]. HFSS solves the problem using FEM methods whereas WASP-NET utilizes MoM together with mode matching techniques. By using these tools, the whole array is analyzed including all effects like mutual coupling. With the obtained results, it is checked whether the array satisfies the design requirements such that the required beam width, side lobe level, input matching etc. If the design does not meet the requirements sufficiently, then fine tuning on the slots must be carried out and the array should be optimized. Fine tuning is done by perturbing the values for the slot offsets and/or lengths by a small amount, then running the simulation once again and checking whether the array performs better than the previous version. The fine tuning process might be especially time consuming if the array is very large. Therefore, it is desirable to have an accurate and efficient simulation tool to ease and accelerate the fine tuning process.

Each of such simulation tools has its own advantage and disadvantages. FEM based solvers are the most accurate and flexible engines; however, in terms of computational efficiency they can be called moderate. They are very fast and efficient especially if the structure of interest has a small volume. However, when the volume gets larger, meshing implemented by the software increases dramatically and much more computational effort must be devoted. In addition, if the surface-

volume ratio of the structure is small like a slotted waveguide array, then MoM based solvers are more efficient than FEM based softwares. As previously stated, in designs where fine tuning is unavoidable, it becomes apparent that the optimization process with FEM solvers gets more and more cumbersome.

On the other hand, softwares like WASP-NET implementing MoM with mode matching techniques to solve the problem, work very well for standard waveguide structures. They are capable of solving several waveguide structures efficiently and accurately. Since they are much faster than a traditional FEM solver, they are preferable when it comes to fine tuning.

The aim of this thesis is to develop a MATLAB [9] executable computer code to analyze a travelling type linear slotted waveguide array with the Method of Moments. The software will be able to analyze slotted waveguide arrays implemented on a standard waveguide, i.e. the waveguide could not be a ridged one and it should not include any kind of irises or insets in the waveguide. In addition, it will not account for wall thickness and it will assume to have square shaped slots rather than rounded slots. As depicted previously, this code will be a building block for a more versatile simulation tool, and it will be open for future modifications, add-ons and improvements.

In Chapter 2, the integral equation formulation to analyze longitudinal slots cut on the broad wall of a standard waveguide will be presented. Then the MoM solution of this integral equation will be explained in detail and similar studies found in the literature will be summarized. In addition, explicit expressions used in the evaluation of the MoM matrix entries will be provided.

In Chapter 3, numerical results obtained by the developed software will be presented. First, results obtained for some canonical problems will be presented to verify that the evaluation of the MoM matrix entries is implemented accurately. Next, the results for the self admittance of a single slot will be presented for different values of

slot offset and length. Finally, the self admittance results will be compared with the measurement results found in the literature.

In Chapter 4, conclusions will be drawn and future works and possible improvements will be discussed.

CHAPTER 2

MOM FORMULATION OF THE SLOTTED WAVEGUIDE ANTENNA ARRAY

2.1. Introduction

Finite Element Method, Method of Moments and mode matching techniques are widely used in the numerical analysis of slotted waveguide antenna arrays. Among these techniques MoM is chosen to be studied in this thesis, because in standard geometries one can write relatively simple and explicit integral equations that can be solved numerically by applying Method of Moments. Effective utilization of MoM yields quite accurate and satisfactory results.

As explained in the previous chapter, Elliott's design methodology of a slotted waveguide antenna array includes the slot characterization conducted either experimentally or numerically, and obtaining the characterization polynomials from the resultant data. In addition, since the remaining design steps are based on the characterization data, the quality and accuracy of these data is of utmost importance. For example, if the resonant length data of the slot has a 2% error, then such an error would cause the array to perform satisfactorily at a different frequency than the design frequency. Furthermore, the array will have a degraded side lobe level as well as a deteriorated input match [10].

To characterize the slot cut on a waveguide, there are two possible ways to do it:

a) Experiments: By manufacturing test waveguides each of which contain a slot of different offset and/or length, and conducting several S-parameter measurements with a vector network analyzer, one can obtain the slot

characterization data. Although this method is also accurate, it is a very expensive and time consuming work. It should be noted that accuracy of this method not only relies on the experiment setup but also on the precision of the manufacturing process.

b) Numerical Analysis: Today, this technique is preferred quite commonly since it gives a fast and accurate way to gather the required data. In the literature, Method of Moments was generally used to obtain these data. Although it brings some restrictions on the problem, it can be said that it is faster, more efficient and less expensive than the previous method. In addition, FEM based tools, are very accurate, flexible and fast especially in solving small structures like the slot cut on a waveguide. By the aid of these sophisticated softwares, obtaining the characterization data in the most accurate and fastest way is possible.

This study will make use of the Method of Moments technique to analyze an array of longitudinal slots cut on the broad wall of the waveguide. In the next subsection the integral equation that models this problem will be presented and the formulation for the MoM solution of this integral equation will be provided.

2.2. Integral Equations and Related Formulations

In this section, the integral equation of slots cut on the broad wall of a waveguide shown in Figure 2-1 will be derived.

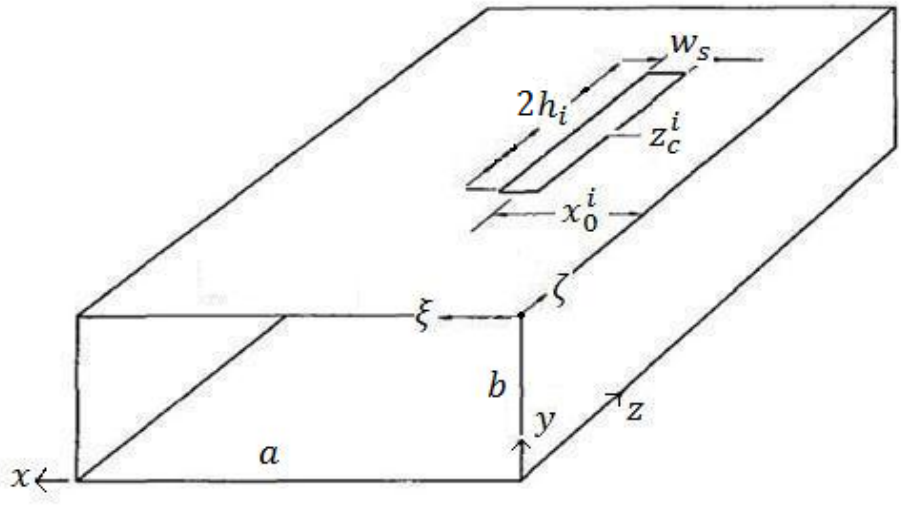

Figure 2-1 Problem geometry for the slot cut on the broad wall of a waveguide.

The integral equation is derived from the boundary condition at the surface of the slot,

$$H_z^{ext}(\xi,\zeta) = H_z^{int}(\xi,\zeta) + H_z^{inc}(\xi,\zeta) \qquad (2\text{-}1)$$

(2-1) shows that the externally scattered H_z-field is equal to the sum of the incident and internally scattered H_z-field. Note that the boundary condition on the other tangential magnetic field (H_x) component could also be taken into account; however, from the study of Elliott and Stern [10], it is understood that this component of the

magnetic field is negligibly small. Therefore, the H_x-field component is discarded throughout the formulation. Consequently, the only tangential component of the electric field will be in x-direction and z-directed electric field will also be neglected at the slot surface. Hence the slot can be modeled with a z-directed magnetic current ($M_z = E_x$) and this magnetic current gives rise to scattered magnetic fields both inside (H^{int}) and outside (H^{ext}) the waveguide. To compute the fields outside the waveguide, the slot will be assumed to be placed on an infinite ground plane.

The incident field is considered to be the dominant mode of the waveguide and the scattered fields can be written in terms of the associated Green's functions. As a result, (2-1) takes the following form:

$$\begin{aligned} H_z^{inc}(\xi,\zeta) &= jA_{10}\cos\left[\frac{\pi}{a}(x_0^i+\xi)\right]e^{-j\beta_{10}\zeta} \\ &= H_z^{ext}(\xi,\zeta) - H_z^{int}(\xi,\zeta) \\ &= \int_{(z_c^i-h_i)}^{(z_c^i+h_i)}\int_{-w_s/2}^{w_s/2} E_x(\xi',\zeta')G(\xi,\zeta;\xi',\zeta')\,d\xi'\,d\zeta' \end{aligned} \tag{2-2}$$

where A_{10} and β_{10} are the amplitude and the propagation constant of the dominant TE_{10} mode, respectively. The Green's function for the combined computation of external and internal fields is

$$\begin{aligned} &G(\xi,\zeta;\xi',\zeta') = \\ &\left(\frac{\partial^2}{\partial\zeta'^2}+\mathrm{k}_0^2\right)\left(\frac{e^{-jk_0R}}{2\pi j\omega\mu_0 R}\right)+\frac{2}{j\omega\mu_0 ab}\sum_{\mathrm{m}=0}^{\infty}\sum_{\mathrm{n}=0}^{\infty}\frac{\epsilon_{\mathrm{mn}}^2}{\gamma_{\mathrm{mn}}}\left\{\cos\left[\frac{m\pi}{a}\left(x_0^j+\xi\right)\right]\cos\left[\frac{m\pi}{a}(x_0^i+\right.\right. \\ &\left.\left.\xi')\right]\left(\frac{\partial^2}{\partial\zeta'^2}+\mathrm{k}_0^2\right)e^{-\gamma_{\mathrm{mn}}|\zeta-\zeta'|}\right\} \end{aligned} \tag{2-3}$$

In (2-3), $\epsilon_{00}^2 = 1/4$, $\epsilon_{\mathrm{m0}}^2 = \epsilon_{\mathrm{n0}}^2 = 1/2, \epsilon_{\mathrm{mn}}^2 = 1$ otherwise. Also $\mathrm{k}_0^2 = \omega^2\mu_0\varepsilon_0$ and

$$\gamma_{\mathrm{mn}} = \sqrt{\left(\frac{m\pi}{a}\right)^2 + \left(\frac{n\pi}{b}\right)^2 - \mathrm{k}_0^2}\,, \qquad (2\text{-}4)$$

$$R = \sqrt{(\xi - \xi')^2 + (\zeta - \zeta')^2}$$

The first part of the summation in (2-3) is the half-space Green's function for the external fields whereas the second part is the Green's function for the fields inside waveguide derived by Stevenson [4]. When examining this equation, it is understood that for the related MoM formulation it is logical to separate it into two parts, namely:

$$G(\xi, \zeta; \xi', \zeta') = G_{ext}(\xi, \zeta; \xi', \zeta') + G_{int}(\xi, \zeta; \xi', \zeta') \qquad (2\text{-}5)$$

$$G_{ext}(\xi, \zeta; \xi', \zeta') = \left(\frac{\partial^2}{\partial \zeta'^2} + \mathrm{k}_0^2\right)\left(\frac{e^{-jk_0 R}}{2\pi j \omega \mu_0 R}\right) \qquad (2\text{-}6)$$

$$G_{int}(\xi, \zeta; \xi', \zeta') = \frac{2}{j\omega\mu_0 ab} \sum_{\mathrm{m}=0}^{\infty} \sum_{\mathrm{n}=0}^{\infty} \frac{\epsilon_{\mathrm{mn}}^2}{\gamma_{\mathrm{mn}}} \left\{ \cos\left[\frac{m\pi}{a}(x_0^j + \xi)\right] \cos\left[\frac{m\pi}{a}(x_0^i + \xi')\right] \left(\frac{\partial^2}{\partial \zeta'^2} + \mathrm{k}_0^2\right) e^{-\gamma_{\mathrm{mn}}|\zeta - \zeta'|} \right\} \qquad (2\text{-}7)$$

The unknown of the integral equation given in (2-2) is the x-directed electric field E_x and as the first step of the MoM procedure it is expanded in terms of piecewise sinusoidal basis functions as:

$$E_x(\xi, \zeta) = \sum_{i=1}^{N} V_i F_i(\zeta) \qquad (2\text{-}8)$$

where $F_n(\zeta)$

$$F_i(\zeta) = \frac{\sin\left(k_0(h_i - |z_c^i - \zeta|)\right)}{\sin(k_0 h_i)} \tag{2-9}$$

In (2-9) k_0 is the free space wave number and z_c^i is the center point of the i^{th} basis function and h_i is the half length of the subdomain for i^{th} basis function as shown in Figure 2-2.

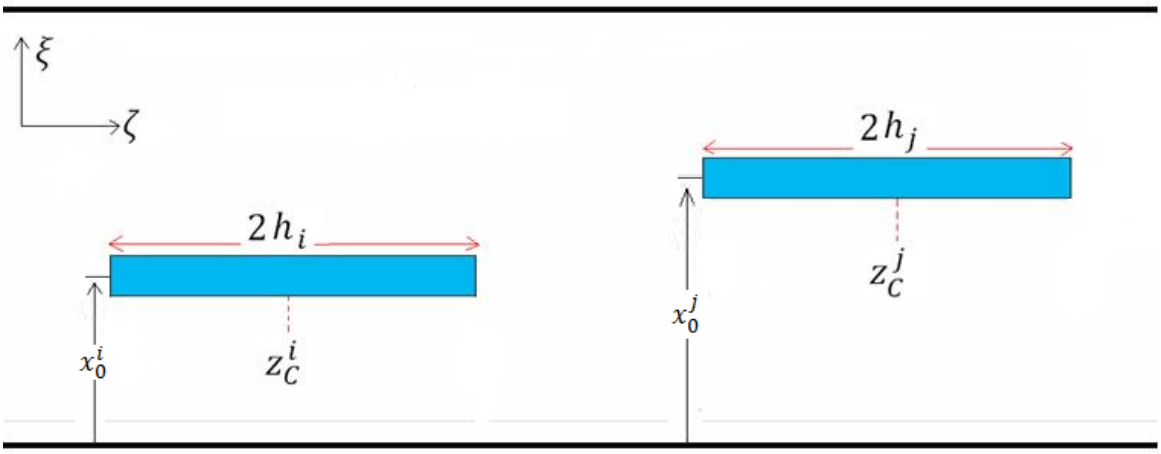

Figure 2-2 The geometry showing the subdomains of i^{th} and j^{th} basis functions

As the next step of the MoM procedure, Galerkin's testing scheme is applied with piecewise sinusoidal weighting functions. The remaining part of the formulation will be presented for the internal and external scattering parts separately in the coming two subsections.

2.2.1. External Scattering Formulations

To simplify the formulation, an external mutual admittance is defined as the inner product integral between the i^{th} basis function and the j^{th} testing function as follows:

$$Y_{ji}^{ext} =< G_{ext} f_i, w_j >;\ i \in [1, \mathrm{N}] \text{ and } j \in [1, \mathrm{N}] \tag{2-10}$$

N is the number of basis functions. For $i \neq j$, (2-10) is explicitly written in [11], i.e.

$$Y_{ji}^{ext} = \frac{j60w_s^2}{\sin(k_0 h_i)\sin(k_0 h_j)} \int_{(z_c^i - h_i)}^{(z_c^i + h_i)} \left(\frac{e^{-jk_0 R_I}}{R_I} + \frac{e^{-jk_0 R_F}}{R_F} - 2\cos k_0 h_j \frac{e^{-jk_0 R_C}}{R_C} \right) \sin k_0 \left(h_i - |z_c^i - \zeta| \right) d\zeta \tag{2-11}$$

Where,

$$R_C = \sqrt{(\xi - \xi')^2 + \left(\zeta - z_c^j\right)^2} \tag{2-12}$$

$$R_I = \sqrt{(\xi - \xi')^2 + \left(\zeta - (z_c^j - h_j)\right)^2} \tag{2-13}$$

$$R_F = \sqrt{(\xi - \xi')^2 + \left(\zeta - (z_c^j + h_j)\right)^2} \tag{2-14}$$

Equation (2-11) is used to numerically calculate Y_{ji}^{ext} in MATLAB environment. Gaussian quadrature is utilized as the numerical integration method.

During the evaluation of the mutual impedance for the self terms, i.e. $i = j$, special care must be taken since the integral involves singularities. Since a center fed dipole antenna and a slot antenna are dual structures, same kind of integrals appear in the formulation of a dipole. Therefore a modified version of the self impedance expression for the center-fed dipole derived by the induced EMF method [11] is utilized for the analytical evaluation of the singular integrals in (2-11) for $i = j$ and the external admittance is expressed as:

$$Y_{ii}^{ext} = \frac{j120w_s^2}{(\sin(k_0h_i)\,\eta)^2}\{4\cos(k_0h_i)^2\,S(k_0h_i) - \cos(2k_0h_i)\,S(2k_0h_i) - \sin(2k_0h_i)[2C(k_0h_i) - C(2k_0h_i)]\} \quad (2\text{-}15)$$

in which

$$C(k_0y) = ln\frac{2y}{w_s} - \frac{1}{2}Cin(2k_0y) - \frac{j}{2}Si(2k_0y) \quad (2\text{-}16)$$

$$S(k_0y) = \frac{1}{2}Si(2k_0y) - \frac{j}{2}Cin(2k_0y) - k_0w_s \quad (2\text{-}17)$$

In (2-16) and (2-17), w_s is the slot width, $Cin(x)$ is the modified cosine integral and $Si(x)$ is the sine integral. η is the free space wave impedance. Both $Si(x)$ and $Cin(x)$ are tabulated functions and they are also available in MATLAB.

2.2.2. Internal Scattering Formulations

2.2.2.1. Internal Scattering Mutual Term Formulation

The internal scattering Green's function given in (2-7) contains derivatives with respect to position. By making use of the properties given in (2-18) for a general Green's function $G(z;z')$, the integral of the sinusoidal basis function and the Green's function with derivatives can be written in the form given in 2-19.

$$\frac{\partial \mathrm{G}}{\partial z'} = -\frac{\partial \mathrm{G}}{\partial \mathrm{z}} \text{ and } \frac{\partial^2 \mathrm{G}}{\partial z'^2} = \frac{\partial^2 \mathrm{G}}{\partial z^2} \tag{2-18}$$

$$\begin{aligned} \frac{1}{\sin(k_0 h)}\left(\frac{\partial^2}{\partial z'^2} + \mathrm{k}_0^2\right) \int_{(z_c-h)}^{(z_c+h)} G(z;z') \sin k_0(h - |z_c - z|)\, dz \\ = \frac{k_0}{\sin(k_0 h)}\{G((z_c - h);z') + G((z_c + h);z') \\ - 2\cos(k_0 h)\, G(z_c;z')\} \end{aligned} \tag{2-19}$$

(2-19) is used to further manipulate (2-7) and obtain the mutual admittance due to the internal coupling Y_{ij}^{int} expression as follows:

$$Y_{ji}^{int} = < G_{int} f_i, w_j > ;\ i \in [1, \mathrm{N}] \text{and } \mathrm{j} \in [1, \mathrm{N}], i \neq j \tag{2-20}$$

$$Y_{ji}^{int} = \frac{2k_0}{j\omega\mu_0 ab\sin(k_0h_i)\sin(k_0h_j)} \sum_{m=0}^{\infty}\sum_{n=0}^{\infty} \frac{\epsilon_{mn}^2}{\gamma_{mn}} I_{ij}^{\xi\xi'}(m) \left\{ \int_{(z_c^i-h_i)}^{(z_c^i+h_i)} \left[G(\zeta;(z_c^j - h_j)) + G(\zeta;(z_c^j + h_j)) - 2\cos(k_0h_j)\, G\left(\zeta; z_c^j\right)\right] \sin k_0\left(h_i - |z_c^i - \zeta|\right) d\zeta \right\} \tag{2-21}$$

$$I_{ji}^{\xi\xi'}(m) = \int_{-w_s/2}^{w_s/2} \int_{-w_s/2}^{w_s/2} cos\left[\frac{m\pi}{a}(x_0^i + \xi)\right] cos\left[\frac{m\pi}{a}(x_0^j + \xi')\right] d\xi d\,\xi' \tag{2-22}$$

$$I_{ji}^{\xi\xi'}(m) = \left(\frac{a}{m\pi}\right)^2 \left\{\sin\left[\frac{m\pi}{a}\left(x_0^i + {w_s}/{2}\right)\right] - \sin\left[\frac{m\pi}{a}\left(x_0^i - {w_s}/{2}\right)\right]\right\}\left\{\sin\left[\frac{m\pi}{a}\left(x_0^j + {w_s}/{2}\right)\right] - \sin\left[\frac{m\pi}{a}\left(x_0^j - {w_s}/{2}\right)\right]\right\}, \text{for } m \neq 0 \tag{2-23}$$

$$I_{ji}^{\xi\xi'}(0) = w_s^2, \qquad \text{for } m = 0 \tag{2-24}$$

in which $I_{ji}^{\xi\xi'}(*)$ denotes the double integral with respect to the $(\xi;\xi')$ variables and

$$G(\zeta;\zeta') = e^{-\gamma_{mn}|\zeta-\zeta'|} \tag{2-25}$$

Again Gaussian quadrature method, as done for the external scattering calculation, is performed to find Y_{ji}^{int} given in expression (2-21).

2.2.2.2. Internal Scattering Self Term Formulation

For the self term calculation, i.e. $i = j$ one cannot use the equation given in (2-21) because of the discontinuity in the derivative of the Green's function in (2-25). Actually, this statement has been verified by comparing the results obtained by the numerical integration of the integral in the left hand side of (2-19) and the analytical evaluation of the right hand side of (2-19). The parameters in Table 2-1 are used during the computations.

Table 2-1 Parameters used for computing (2-19)

Parameters	Value
$G(z;z')$ $= e^{-\gamma_{10}\lvert z-z'\rvert}$	TE_{10} Mode $\gamma_{10} = j140.36\, rad/m$
f	$9.375GHz$
k_0	$196.43\, rad/m$
$2h$	$0.0140m$
z_c	$0.0070m$
z'	$[-0.04, 0.04]m$ $201\ points$

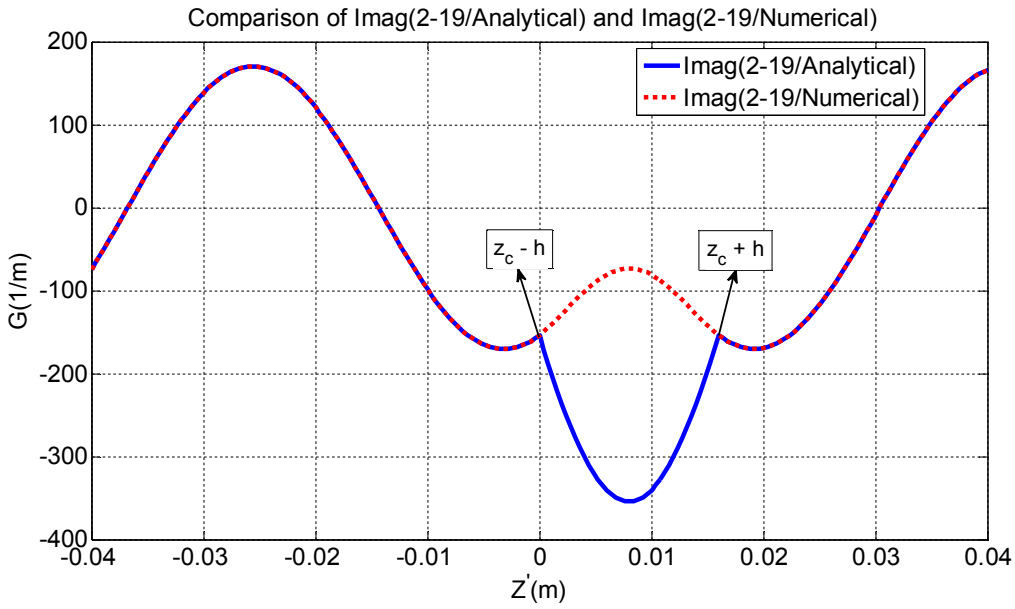

Figure 2-3 Plot of the imaginary parts of (2-19/Analytical) and (2-19/Numerical).

The imaginary parts of the numerical and analytical results are plotted in Figure 2-3. It is clearly seen that the results do not match in $z' \in (z_c - h,\ z_c + h)$ region. Thus it is evident that the formulation in (2-21) cannot be used in the internal scattering self term calculation.

On the other hand, if one attempts to implement (2-7) directly in the MoM formulation instead of using (2-19), s/he will end up with the convergence problems associated with the summation of the modes. Next, the convergence problems encountered during this direct evaluation of (2-7) will be summarized. First of all, substituting (2-7) in the MoM equation, one gets the following:

$$Y_{ji}^{int} = < G_{int} f_i, w_j >;\ i,j \in [1,N], i = j \qquad (2\text{-}26)$$

$$Y_{ii}^{int}$$

$$= \frac{2}{j\omega\mu_0 ab\sin(k_0 h_i)^2} \sum_{m=0}^{\infty}\sum_{n=0}^{\infty} \frac{\epsilon_{mn}^2(\gamma_{mn}^2 + k_0^2)}{\gamma_{mn}} I_{ii}^{\xi\xi'}(m) \left\{ \iint_{(z_c^i - h_i)}^{(z_c^i + h_i)} \sin k_0\big(h_i - \big|z_c^i - \zeta\big|\big) \sin k_0\big(h_i - \big|z_c^i - \zeta'\big|\big) e^{-\gamma_{mn}|\zeta - \zeta'|} d\zeta d\zeta' \right\} \quad (2\text{-}27)$$

$$I_{ii}^{\xi\xi'}(m) = \left(\frac{a}{m\pi}\right)^2 \left\{ \sin\left[\frac{m\pi}{a}\left(x_0^i + {}^{w_s}/_2\right)\right] - \sin\left[\frac{m\pi}{a}\left(x_0^i - {}^{w_s}/_2\right)\right] \right\}^2, for\ m \neq 0 \quad (2\text{-}28)$$

$$I_{ii}^{\xi\xi'}(0) = w_s^2, \qquad for\ m = 0 \quad (2\text{-}29)$$

(2-27) is implemented in MATLAB with the parameters in Table 2-2 and plotted the imaginary parts of Y_{11} internal scattering for each TE_{mn} mode in Figures 2-4 and 2-5. Both the numerical and analytical integration methods have been used to implement (2-27) and the two methods resulted in exactly the same results.

Table 2-2 Parameters used for implementing (2-27)

Parameters	Value
f	$9.375GHz$
k_0	$196.43\ rad/m$
a	$0.0229m$
b	$0.0102m$
$2h$	$0.0140m$
z_c	$0.0070m$
m	$[1,50]$
n	$[1,50]$

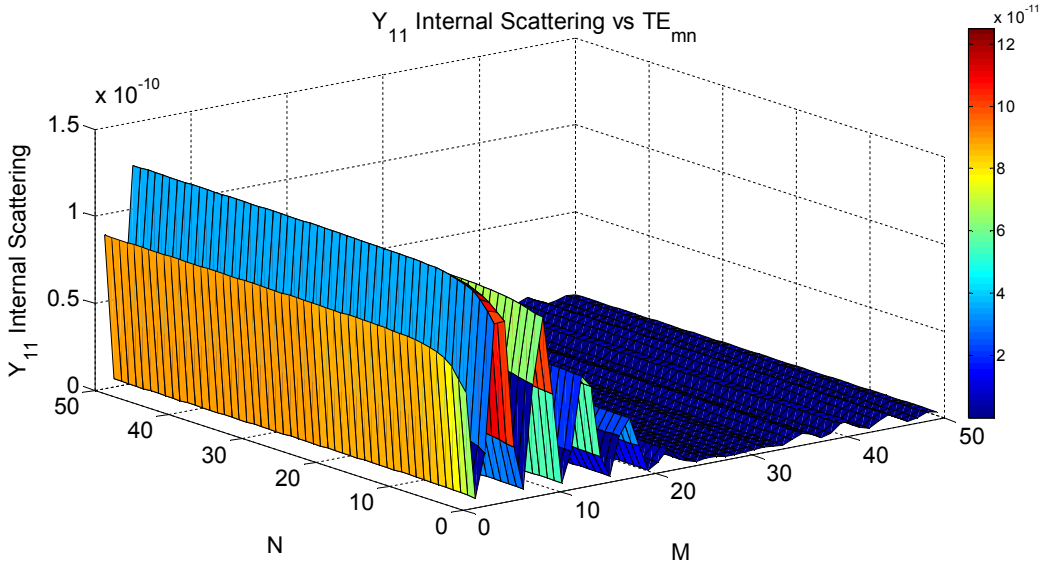

Figure 2-4 Imag(Y_{11}) vs TE_{mn} Modes computed using (2-27).

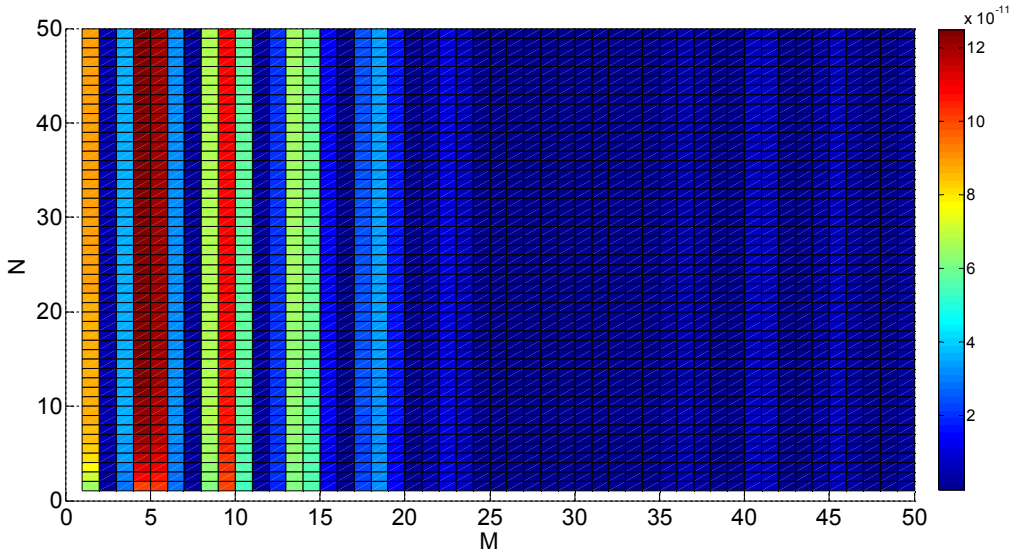

Figure 2-5 Imag(Y_{11}) vs TE_{mn} Modes computed using (2-27).(XY View)

From the Figures 2-4 and 2-5 it is clearly observed that along the N-modes Y_{11} does not decay. This means, if all the Y_{11} terms corresponding to each TE_{mn} mode are summed up, the summation will diverge. Another interesting feature that is seen from Figure 2-5, is that along the M-modes the decay is not exactly exponential, indeed the maximum of Y_{11} occurs at TE_{5n} and this is due to the effect of the $I_{ii}^{\xi\xi'}$ integral shown in (2-28). In fact, this shows that the reactive power contribution of TE_{5n} is higher than that of for instance TE_{2n} modes.

To overcome the convergence problem, the integral given in (2-7) needs to be computed with a different approach. While exploring a new approach, it is realized that the derivatives acting on the Green's function could be transferred on the basis and testing functions by using the following relations:

$$\iint_{(z_c-h)}^{(z_c+h)} \frac{\partial^2 G(z;z')}{\partial z'^2} f(z)g(z')\,dz\,dz' = -\iint_{(z_c-h)}^{(z_c+h)} G(z;z')\frac{df(z)}{dz}\frac{dg(z')}{dz'}\,dz\,dz' \tag{2-30}$$

$$f(z_c-h) = f(z_c+h) = g(z_c-h) = g(z_c+h) = 0 \tag{2-31}$$

When the integrals are transferred on the basis and testing functions, the integration domain needs to be segmented into four regions as shown in Figure 2-6, due to the absolute value appearing in the argument of piecewise sinusoidal functions. In Figure 2-6, horizontal axis represents the position along the basis function and the vertical axis represents the position along the testing function. In regions (a) and (d) the derivatives of the basis function involves a negative sign due to the absolute value whereas the sign is positive in regions (b) and (c) for the derivatives on the basis function. Similar discussions are valid for the testing function such that positive derivative for regions (c) and (d) and negative for (a) and (b). Hence the overall result will be different in these four different regions.

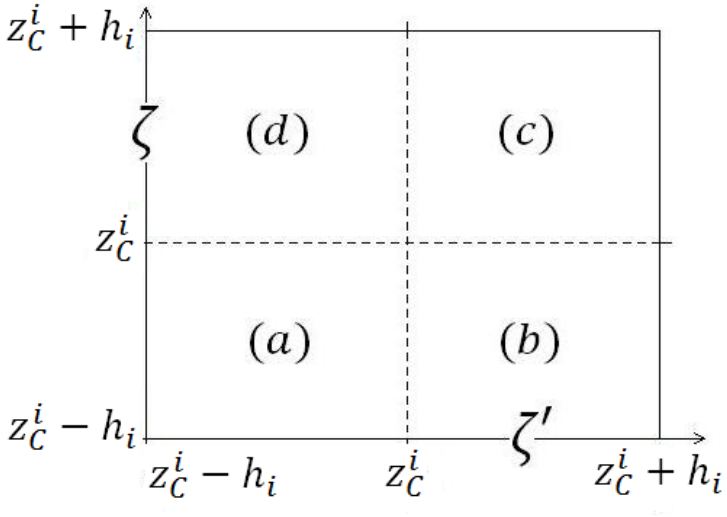

Figure 2-6 Problem geometry for the self term calculation

Using (2-30), the second order derivative applying onto $e^{-\gamma_{mn}|z-z'|}$ is removed and transported to the basis and the testing functions via integration by parts for each region as shown in (2-32) thru (2-36).

$$Y_{ii}^{int(a)} = \frac{-2}{j\omega\mu_0 ab\sin(k_0 h_i)^2} \sum_{m=0}^{\infty}\sum_{n=0}^{\infty} \frac{\epsilon_{mn}^2 k_0^2}{\gamma_{mn}} I_{ii}^{\xi\xi'}(m) \left\{ \int_{(z_c^i - h_i)}^{z_c^i} \int_{(z_c^i - h_i)}^{z_c^i} \cos k_0(h_i - (z_c^i - \zeta)) \cos k_0\big(h_i - (z_c^i - \zeta')\big) e^{-\gamma_{mn}|\zeta - \zeta'|} d\zeta d\zeta' \right\} \quad (2\text{-}32)$$

$$Y_{ii}^{int(b)}$$

$$= \frac{+2}{j\omega\mu_0 ab\sin(k_0 h_i)^2} \sum_{m=0}^{\infty}\sum_{n=0}^{\infty} \frac{\epsilon_{mn}^2 k_0^2}{\gamma_{mn}} I_{ii}^{\xi\xi'}(m) \left\{ \int_{(z_c^i - h_i)}^{z_c^i} \int_{z_c^i}^{(z_c^i + h_i)} \cos k_0\big(h_i - (z_c^i - \zeta)\big) \cos k_0\big(h_i + (z_c^i - \zeta')\big) e^{-\gamma_{mn}|\zeta - \zeta'|} d\zeta d\zeta' \right\} \quad (2\text{-}33)$$

$$Y_{ii}^{int(c)}$$

$$= \frac{-2}{j\omega\mu_0 ab\sin(k_0 h_i)^2} \sum_{m=0}^{\infty}\sum_{n=0}^{\infty} \frac{\epsilon_{mn}^2 k_0^2}{\gamma_{mn}} I_{ii}^{\xi\xi'}(m) \left\{ \int_{z_F^i}^{(z_c^i + h_i)} \int_{z_c^i}^{(z_c^i + h_i)} \cos k_0\big(h_i + (z_c^i - \zeta)\big) \cos k_0\big(h_i + (z_c^i - \zeta')\big) e^{-\gamma_{mn}|\zeta - \zeta'|} d\zeta d\zeta' \right\} \quad (2\text{-}34)$$

$$Y_{ii}^{int(d)}$$

$$= \frac{+2}{j\omega\mu_0 ab\sin(k_0 h_i)^2} \sum_{m=0}^{\infty}\sum_{n=0}^{\infty} \frac{\epsilon_{mn}^2 k_0^2}{\gamma_{mn}} I_{ii}^{\xi\xi'}(m) \left\{ \int_{z_c^i}^{(z_c^i + h_i)} \int_{(z_c^i - h_i)}^{z_c^i} \cos k_0\big(h_i + (z_c^i - \zeta)\big) \cos k_0\big(h_i - (z_c^i - \zeta')\big) e^{-\gamma_{mn}|\zeta - \zeta'|} d\zeta d\zeta' \right\} \quad (2\text{-}35)$$

$$Y_{ii}^{int} = Y_{ii}^{int(a)} + Y_{ii}^{int(b)} + Y_{ii}^{int(c)} + Y_{ii}^{int(d)} \quad (2\text{-}36)$$

The preceding formulations are implemented in MATLAB with the parameters given in Table 2-2. The results are plotted in Figures 2-7 and 2-8.

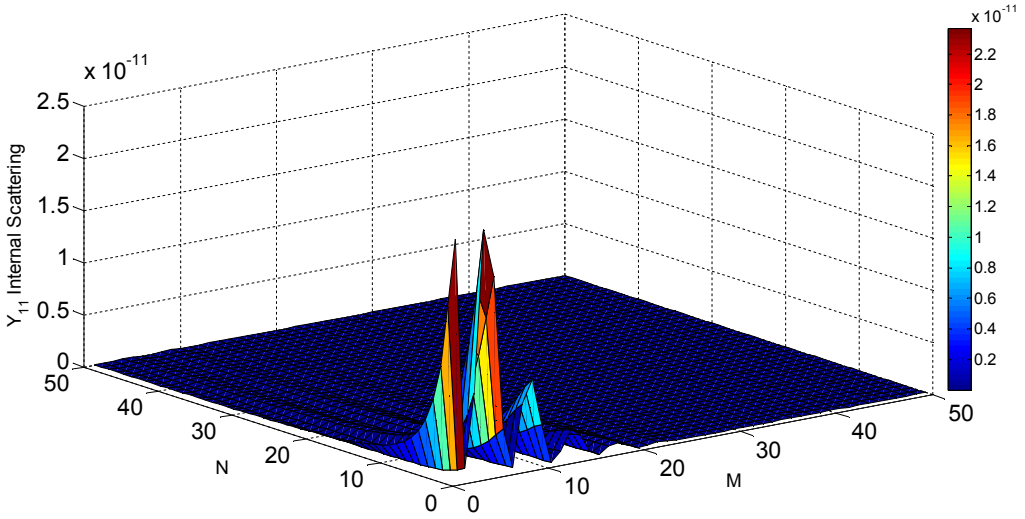

Figure 2-7 Imag(Y_{11}) vs TE_{mn} Modes computed using (2-36).

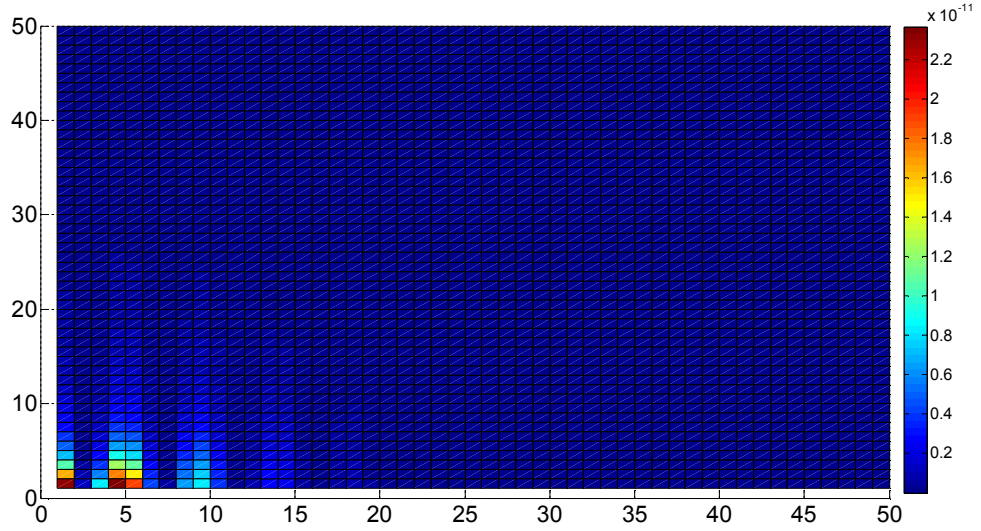

Figure 2-8 Imag(Y_{11}) vs TE_{mn} Modes computed using (2-36).(XY View)

From Figures 2-7 and 2-8, it is clearly seen that the convergence problem observed in Figures 2-4 and 2-5 is solved. Both in the M and N-modes the decaying behavior is apparently observed which means that the infinite mode summation has become now a convergent series. Therefore, the internal scattering self term can be computed using (2-32) thru (2-36).

2.2.3. Computation of the Excitation Vector in the MoM Formulation

In the preceding subsections the expressions for the computation of the MoM matrix entries are presented. In this subsection the computation of the excitation vector will be provided. The excitation vector can be found from the inner product integral of the incident field and the testing functions. Hence the i^{th} entry of the excitation vector denoted by I can be written as:

$$I_i = jA_{10}\frac{a}{\pi}\left\{\sin\left[\frac{\pi}{a}\left(x_0^i + {}^{w_s}/_2\right)\right] - \sin\left[\frac{\pi}{a}\left(x_0^i - {}^{w_s}/_2\right)\right]\right\} * \int_{(z_c^i - h_i)}^{(z_c^i + h_i)} e^{-j\beta_{10}(\zeta - z_c^i)} \sin k_0\left(h_i - |z_c^i - \zeta|\right) d\zeta \qquad (2\text{-}37)$$

The overall MoM matrix will be the summation of internal and external admittance matrices
($Y_{ij} = Y_{ij}^{int} + Y_{ij}^{ext}$) and the matrix equation to be solved for the unknown slot voltages (i.e. V_i's) can be written as:

$$\boldsymbol{I} = \boldsymbol{Y} * \boldsymbol{V} \qquad (2\text{-}38)$$

2.3. Conclusion

In this chapter, the integral equations for the MoM solution are presented. Both the internal and external scattering admittance calculations are performed in MATLAB environment. In the cases where numerical integration is needed, Gaussian quadrature has been used as the numerical integration method. The major difficulty is encountered in the internal scattering self term computation. As described earlier, the infinite mode series in (2-27) inherently does not converge because of the second order derivative; therefore, one needs to transfer this derivative to the basis and testing functions to obtain a convergent summation.

CHAPTER 3

NUMERICAL RESULTS

3.1. Introduction

In the previous chapter, the related integral equations to be used in the MoM solution have been developed. In this chapter, the solver will be verified by analyzing a single slot and comparing the self admittance results with the experimental results obtained by Stegen [5].

3.2. External Scattering Impedance Calculation

3.2.1. External Scattering Self Impedance Calculation

In Elliott's book the self impedance of a center-fed dipole is investigated thoroughly with different approaches such as the induced EMF method and Storer's variational solution [11]. The self impedance results for a dipole can be used to test the self term of the external admittance matrix in our formulation since dipole and slot are dual structures and the dipole impedance is related to slot admittance through Booker's relation [2]. The self impedance of a center-fed dipole with respect to the dipole length is plotted for 5 different dipole radii in Figure 3-1 (Taken from [11]). We converted this problem to the complementary case of the dipole, i.e. a slot with different slot width values. In Figure 3-2 the susceptance of a slot, due to the external scattering, for different slot width cases can be observed and they are in agreement with the ones seen in Figure 3-1. Furthermore, the conductance of this slot for

different slot widths is shown in Figure 3-3. As seen from both Figures 3-1 and 3-3, the conductance of a slot is independent of its width like the resistance of a center-fed dipole is independent of the dipole radius. The agreement between Figure 3-1 and Figures 3-2 and 3-3 verifies that the computation of the self term for the external admittance matrix is performed accurately. In the next subsection, the verification for the accurate implementation of the external admittance matrix for the entries other than the self term will be studied.

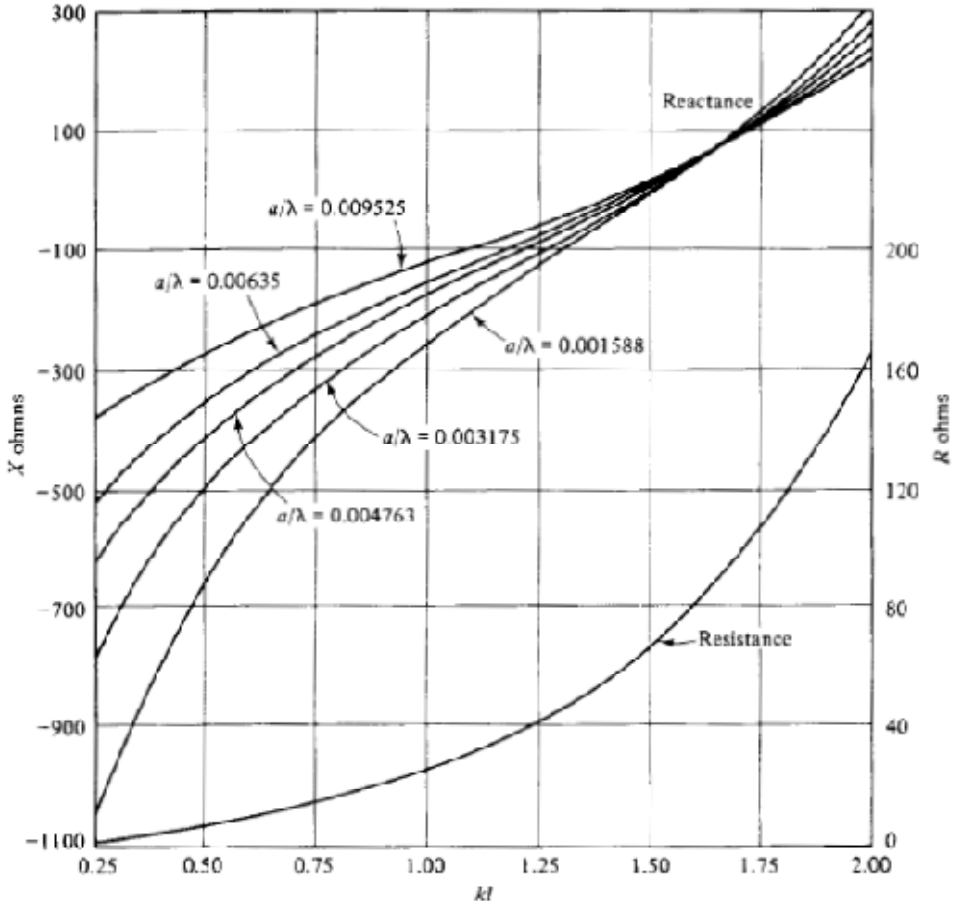

Figure 3-1 Self impedance graphs in Elliott's book [11]. Plotted for five different dipole radii.

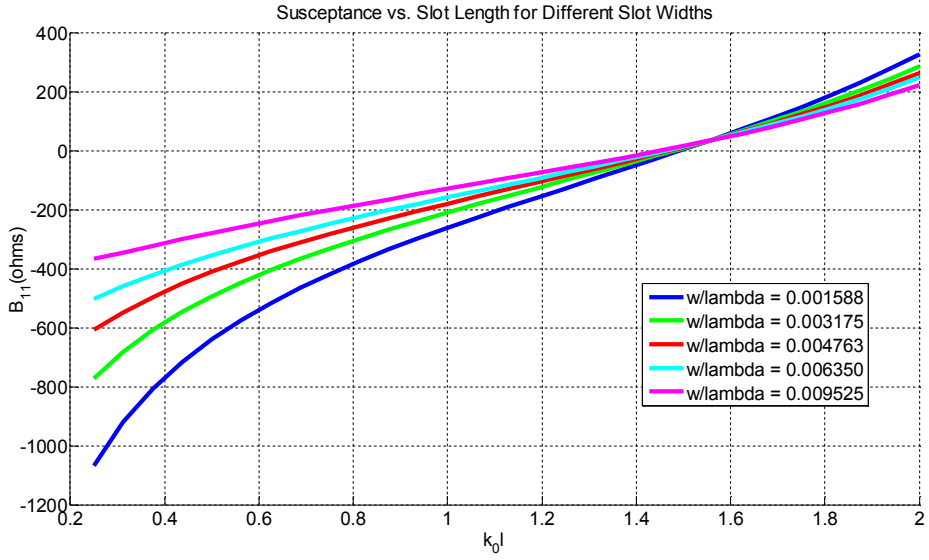

Figure 3-2 Self susceptance graphs for different slot widths obtained from the code.

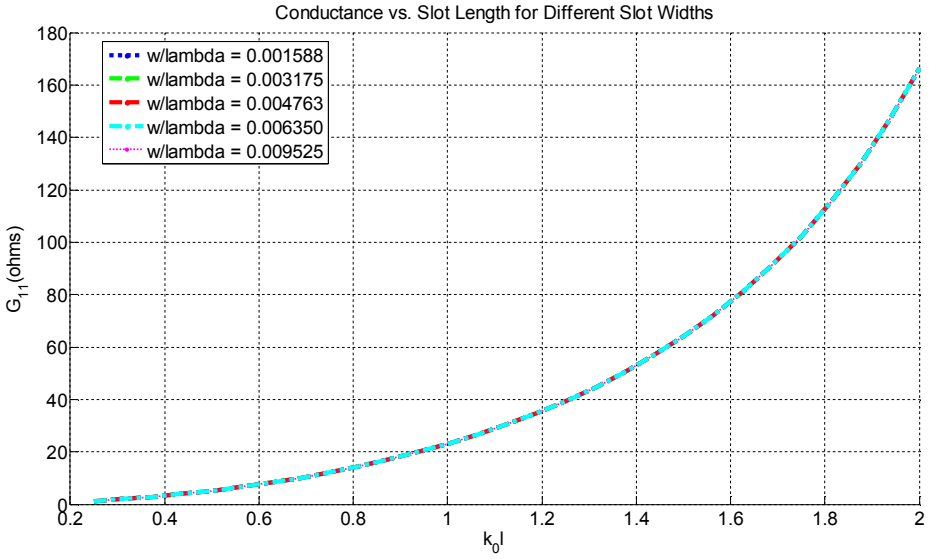

Figure 3-3 Self conductance graphs for different slot widths obtained from the code.

3.2.2. External Scattering Mutual Impedance Calculation

In Elliott's book the problem of finding the mutual impedance of two dipoles shown in Figure 3-4 is again very similar to the mutual impedance of two slots due to external scattering. Therefore, we adopted the equations with small modifications and converted it to the problem of the external mutual admittance of two slots. In Figure 3-5, Figure 3-7 and Figure 3-9, the variation of R_{12} and X_{12} (real and imaginary parts of the mutual impedance) with the separation distance is plotted for three different dipole lengths (Taken from [11]). To verify our approach, the external admittance for two slots with the same parameters as the dipoles are calculated and Figure 3-6, Figure 3-8 and Figure 3-10 show us how G_{12} and B_{12} varies with respect to separation distance for three different slot lengths. Figures 3-5 and 3-6 show the results for the side by side configuration of the dipoles and the slots, respectively. The results are repeated for a cross configuration and the dipole and slot results are presented in Figures 3-7 and 3-8, respectively. Finally, the computations are carried out for an end to end configuration and the dipole and slot results are presented in Figures 3-9 and 3-10, respectively.

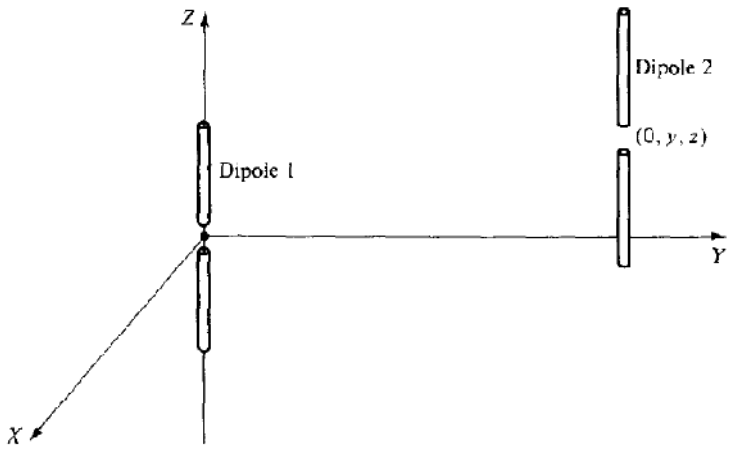

Figure 3-4 Two parallel dipoles for which mutual impedance will be calculated [11].

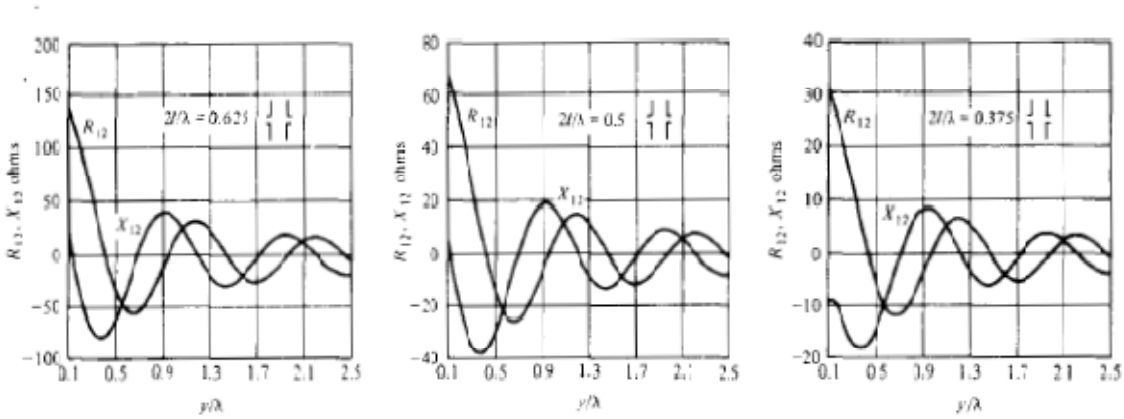

Figure 3-5 The mutual impedance between two dipoles for the side by side configuration [11].

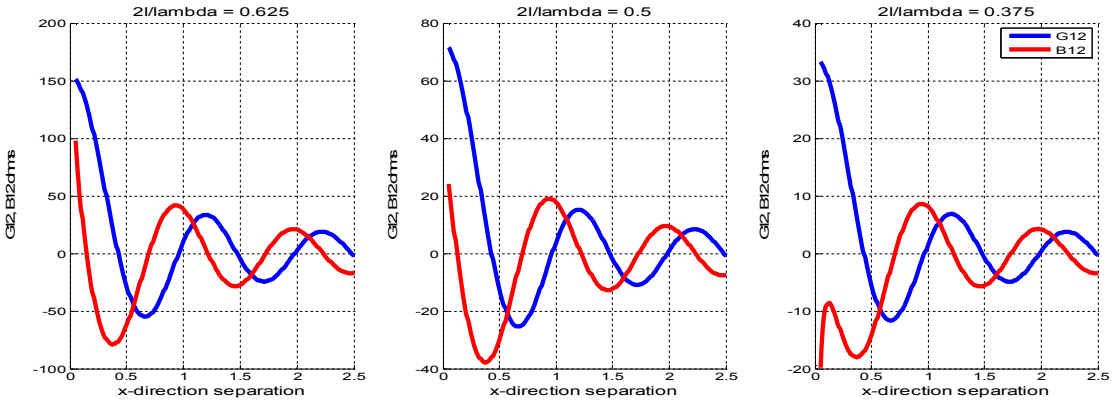

Figure 3-6 The mutual external admittance between two slots for the side by side configuration.

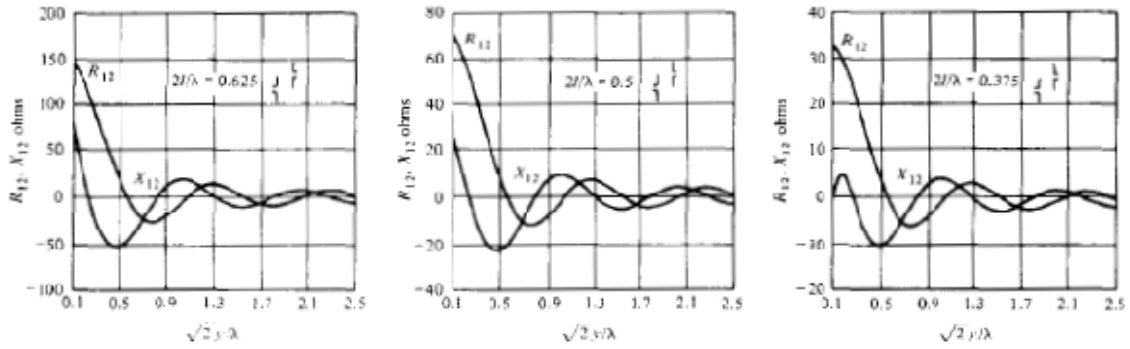

Figure 3-7 The mutual impedance between two dipoles for the cross configuration [11].

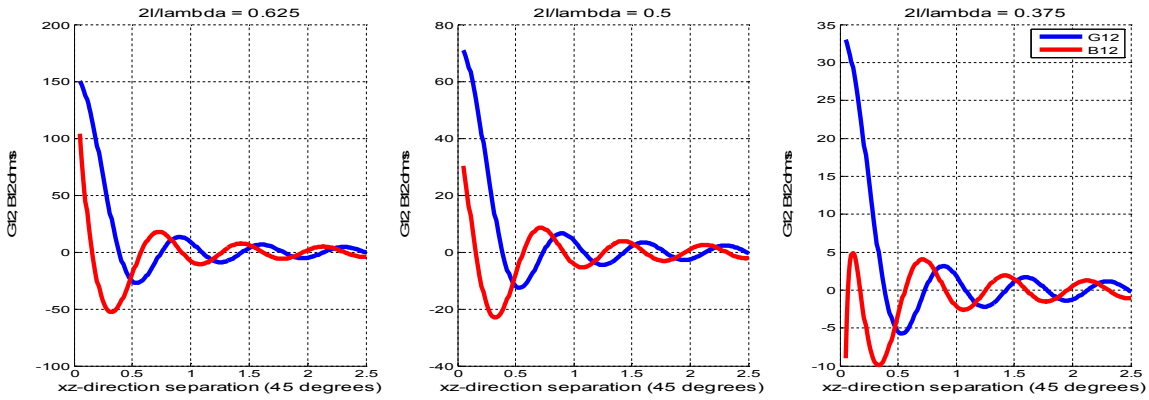

Figure 3-8 The mutual external admittance between two slots for the cross configuration.

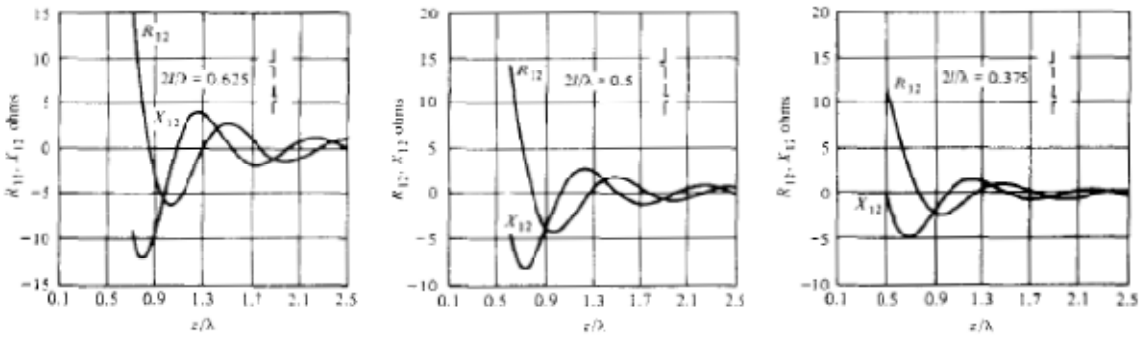

Figure 3-9 The mutual impedance between two dipoles for the end to end configuration [11].

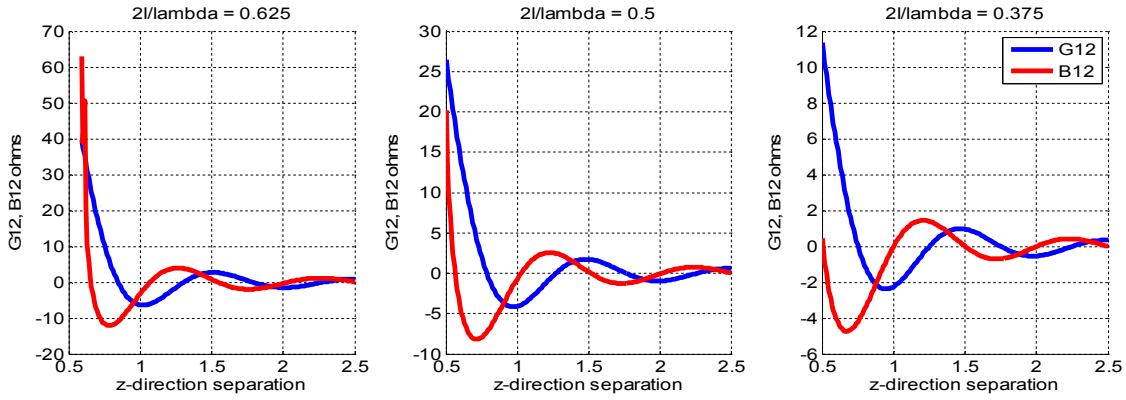

Figure 3-10 The mutual external admittance between two slots for the end to end configuration.

Comparing Figure 3-5, Figure 3-7 and Figure 3-9 with Figure 3-6, Figure 3-8 and Figure 3-10, it can be observed that the results are in very good agreement. This comparison verifies that the external admittance formulation is accurately implemented for the entries of the admittance matrix other than the self term as well.

3.2.3. Self Admittance of a Single Slot on a Waveguide

In this section, we will analyze a single isolated slot with the developed software and obtain the admittance characteristics of the slot for several slot offsets and compare the results with the ones gathered experimentally by Stegen [5]. The initial analysis is performed with a single basis function on the slot, then it is extended to consider several basis functions. The related code built on the MoM formulations explained in the previous chapter runs as indicated in the following steps:

a) Set the relevant parameters like frequency(ω), waveguide dimensions(a, b), slot offset(x_0), slot length($2h$) etc.

b) Given the parameters find Y_{11}^{ext} using (2-15), Y_{11}^{int} utilizing (2-36) and Y_1^{inc} solving (2-37). Afterwards applying (2-38) one finds V_1, the coefficient of the basis function, i.e. the electric field represented by the piecewise sinusoid given in (2-9).

c) Having found the electric field in the slot, compute the backscattered field B_{10} of the dominant mode TE_{10} using:

$$B_{10} = \frac{2V_1}{j\omega\mu_0 ab\left(\frac{\beta_{10}}{k_0}\right)}(\cos\beta_{10}h - \cos k_0 h)\cos\frac{\pi x_0}{a} \qquad (3\text{-}1)$$

d) From B_{10}, Y/G_0 can readily be calculated using (3-2) as follows:

$$\frac{Y}{G_0} = -\frac{2B_{10}}{A_{10} + B_{10}} \tag{3-2}$$

e) In (3-2), A_{10} can be set to 1 for simplicity and without loss in generality.

f) The resonant length of the slot is defined when $^{Y}/_{G_0}$ is purely real. So sweep the slot length within a predefined interval and at each slot length calculate the $^{Y}/_{G_0}$ ratio. Check whether $^{Y}/_{G_0}$ is purely real, i.e. the imaginary part is nearly zero.

The above described procedure has been followed with the parameters given in Table 3-1 and the results have been compared with the ones obtained by Stegen [5].

Table 3-1 Parameters used to obtain the Stegen's Curves

Parameters	Value
f	$9.375GHz$
k_0	$196.43\ rad/m$
a	$0.0229m$
b	$0.0102m$
x_0	$[0.05, 0.10, 0.15, 0.20, 0.25]inch$
z_c	$0m$
$2h$	$[0.0070, 0.0180]m$ & $201points$

Table 3-1 (Continued)

m	$[5, 10, 20, 40]$
n	$[5, 10, 20, 40]$
Total Number of Modes: $(m+1)*(n+1)-1$	$[35, 120, 440, 1680]$

In Figure 3-11 G_r/G_0 is plotted, i.e. the normalized resonant conductance with respect to several slot offsets. Note that the internal Green's function involves an infinite series summation over the waveguide modes.

In order to investigate the effects of truncating this series at a certain number of modes, the calculations are repeated for different number of modes (m and n). The results are plotted in Figure 3-11. In Figure 3-12 the curve obtained by Stegen's experiments can be seen. The results seem to be consistent.

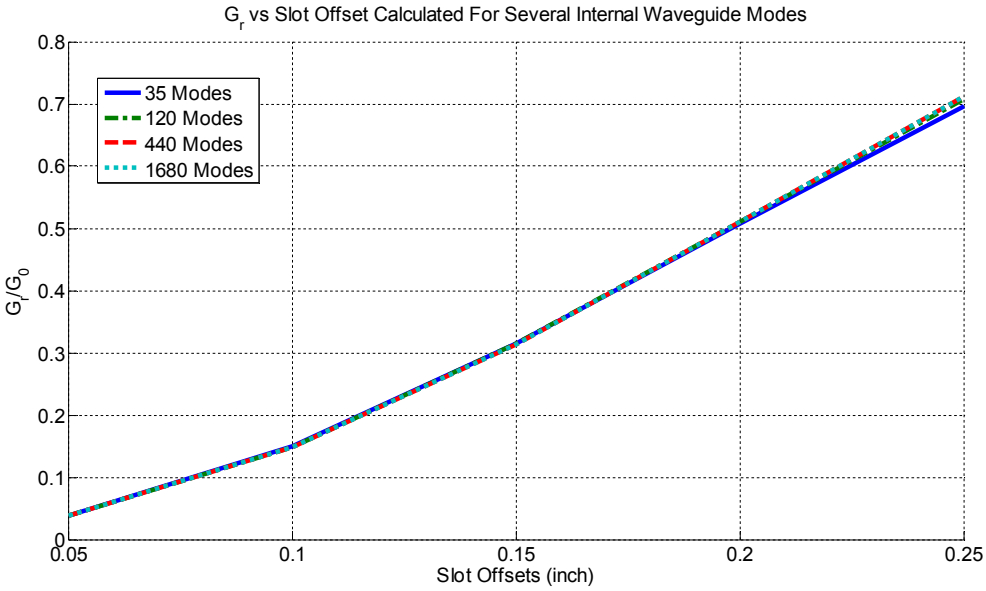

Figure 3-11 G_r/G_0 obtained from the software for different slot offsets.

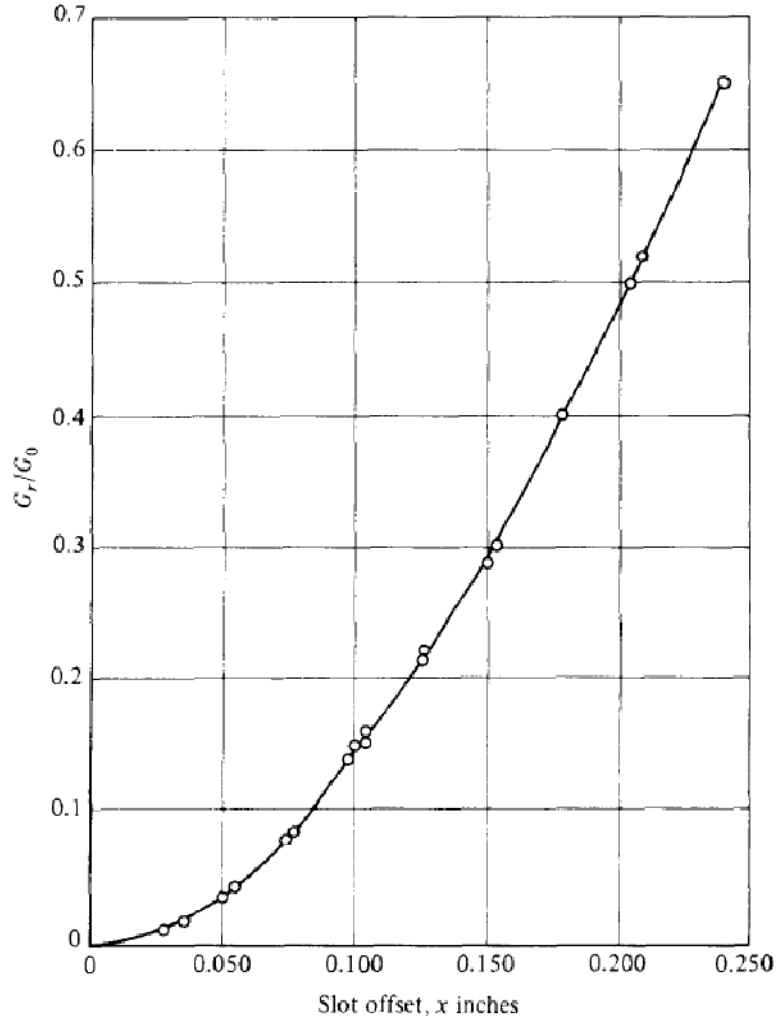

Figure 3-12 G_r/G_0 obtained from Stegen's experimental data.

In Figure 3-11, it is seen that as the number of internal waveguide modes is increased, the resonant conductance does not change at all. This is an expected behavior because the real power present in the slot is mainly due to the internally scattered TE_{10} mode and the externally scattered field. Furthermore, comparing Figures 3-11 and 3-12, it is observed that the two curves track each other very well.

In Figure 3-13 $k_0 l_r$ is plotted, i.e. the resonant length with respect to several slot offsets. In Figure 3-14 the curve obtained by Stegen's experiments can be seen.

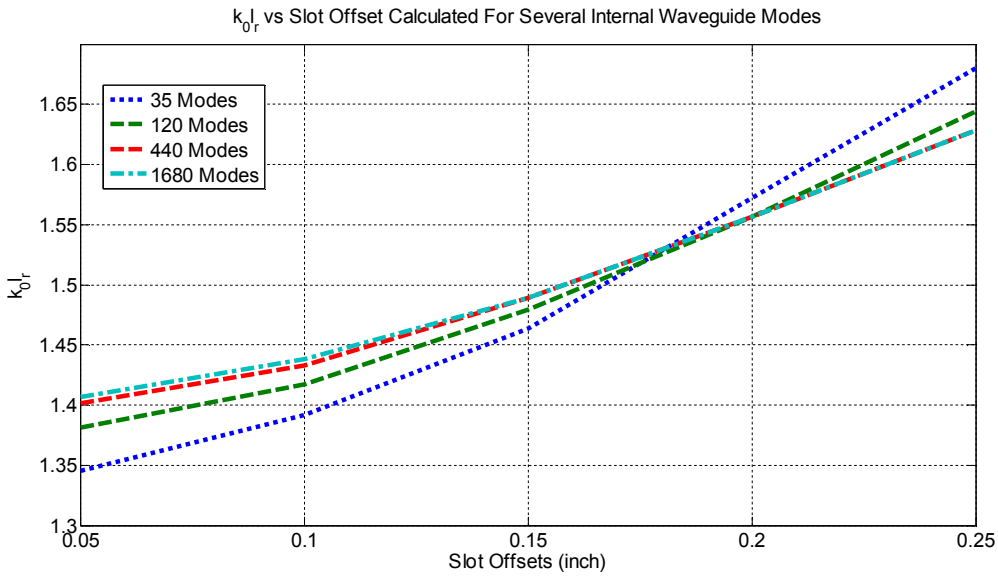

Figure 3-13Variation of $k_0 l_r$ with slot offset, calculated for different number of internal scattering modes.

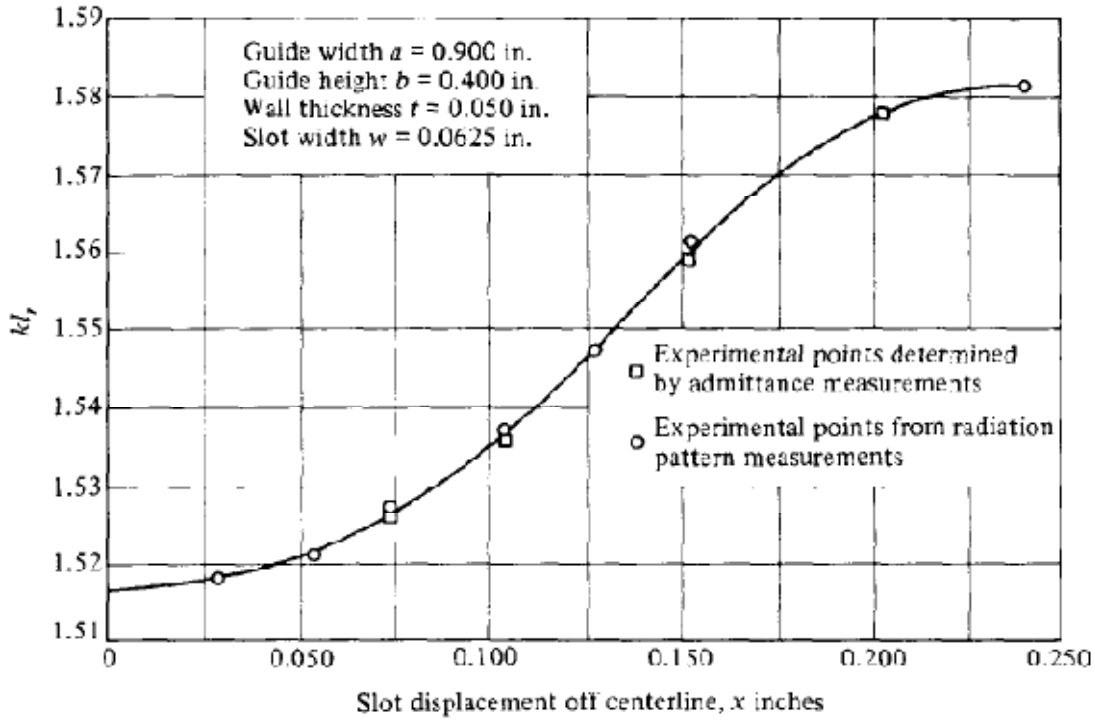

Figure 3-14 $k_0 l_r$ obtained from Stegen's experimental data.

In Figure 3-13, the resonant length does not change very much as the mode number that is taken into account increases. In fact, the resonant length calculated for 440 and 1680 number of modes is nearly the same. Although the internal scattering waveguide modes -except the TE_{10} mode- involved in the resonant length calculation are evanescent modes, they have an important contribution to the reactive power present in the slot. Therefore, even though the real part of the slot admittance is barely affected from these evanescent modes, the imaginary part of the slot admittance changes which results in the change of the resonant length.

From the preceding figures, it is understood that the resonant length behavior converges when 440 number of internal waveguide modes are taken into account.

Therefore, it is decided to proceed the analysis with the 440 number of internal waveguide modes. In Figures 3-15 and 3-16 the conductance and susceptance normalized with respect to the conductance at the resonant length is plotted against the slot length normalized with respect to the resonant length. In Figure 3-19 the curve obtained by Stegen's experiments is present.

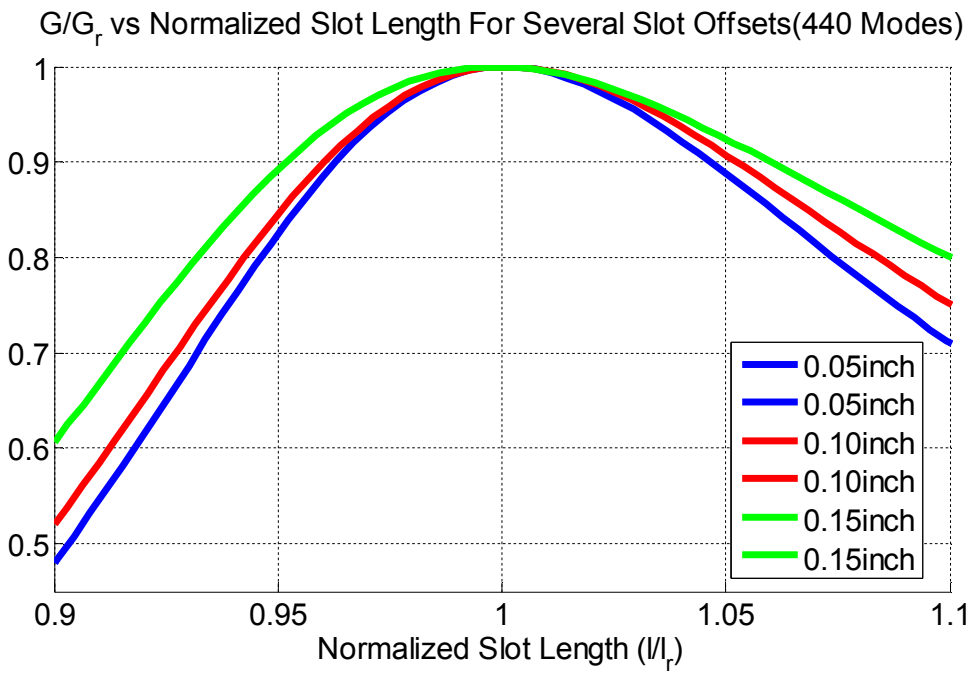

Figure 3-15 Normalized conductance(G/G_r) vs normalized slot length(l/l_r) for different slot offsets. Internal waveguide modes summed up to TE_{2020} (Total Number of Modes = 440).

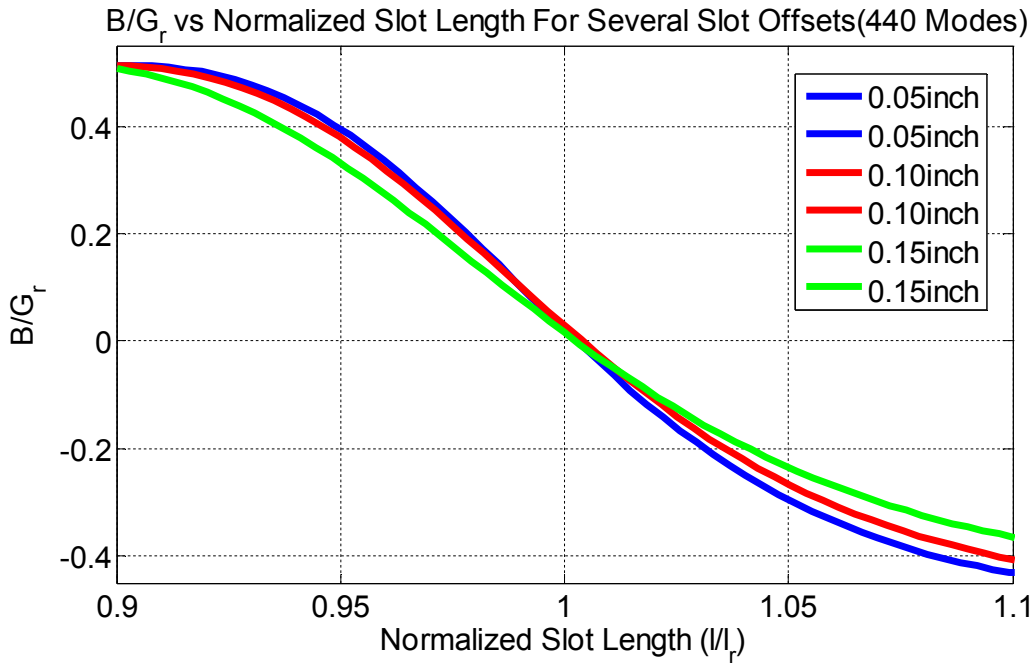

Figure 3-16 Normalized susceptance(B/G_r) vs normalized slot length(l/l_r) for different slot offsets. Internal waveguide modes summed up to TE_{2020} (Total Number of Modes = 440).

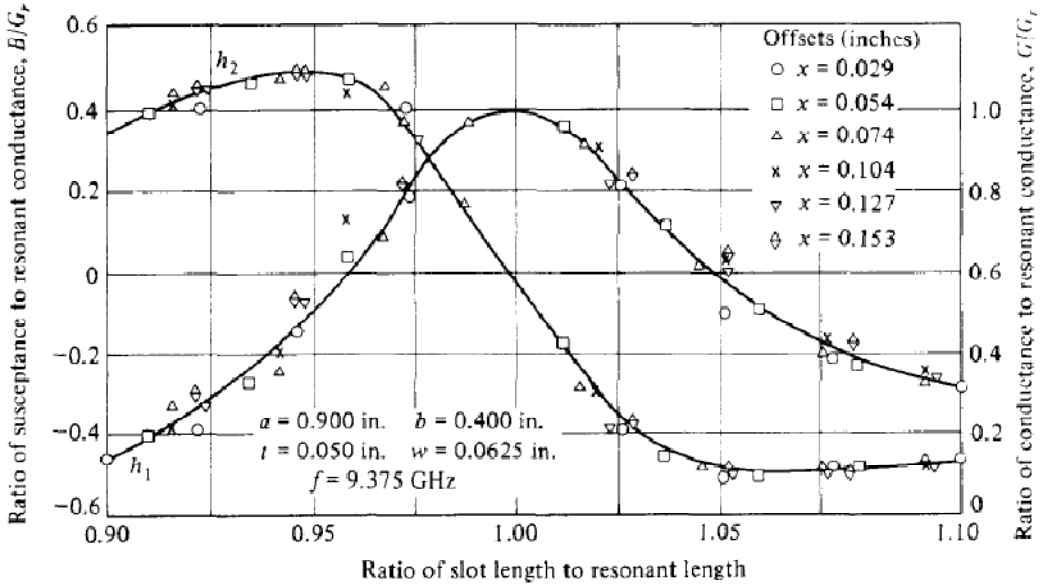

Figure 3-17 Normalized admittance($G/G_r, B/G_r$) vs normalized slot length(l/l_r) for different slot offsets. Obtained from Stegen's experimental data [11].

Comparing Figures 3-15 and 3-16 with Figure 3-17, a fair agreement can be observed. The discrepancy between these curves is due to the fact that the analysis is conducted with a single basis function. Therefore, this difference present in the preceding analysis is acceptable.

Lastly, for the single slot, the number of basis functions has been increased to five and the electric field has been computed with the parameters given in Table 3-2. The result is plotted in Figure 3-18 for $N = 1$ and $N = 5$.

Table 3-2 Parameters used to compute the E_x-field along the slot

Parameters	Value
f	$9.375GHz$
k_0	$196.43\ rad/m$
a	$0.0229m$
b	$0.0102m$
x_0	$0.15inch$
z_c	$0m$
$2h$	$0.0156m$
m	25
n	25
N (Number of Basis Functions)	$[1, 5]$

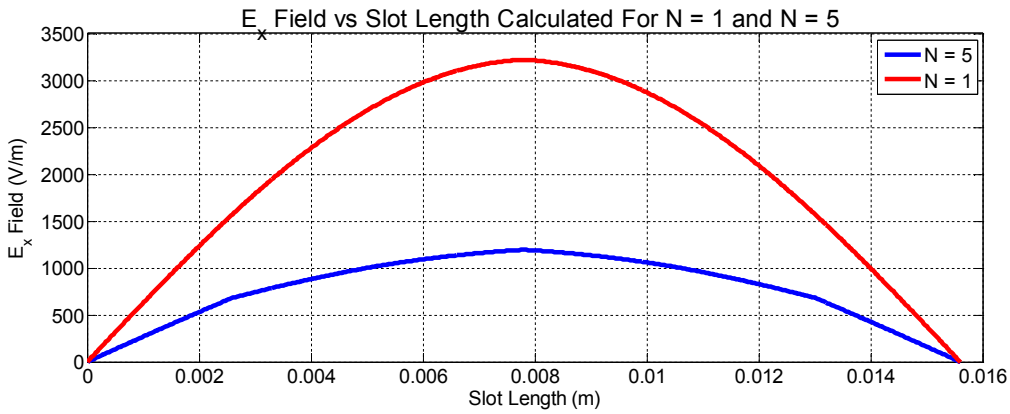

Figure 3-18 Computed E_x-field along the slot for N = 1 and N = 5.

From Figure 3-18, it is observed that the electric field across the slot has a piecewise sinusoidal behavior as expected for both $N = 1$ and $N = 5$. Nevertheless, for the $N = 5$ case, the peak value of the electric field across the slot decreases to the one-third of the $N = 1$ case. The main cause of this error is possibly due to some mistakes present in the developed code.

3.3. Conclusion

In this chapter the numerical results obtained from the MoM solution of a slot cut on the broad wall of a waveguide has been presented. Firstly, the external scattering equations obtained in Chapter 2 have been implemented in MATLAB. Since a slot cut on an infinite ground plane and a center-fed dipole are dual structures, the external mutual and self admittance characteristics of a slot should be similar to the mutual and self impedance characteristics of a dipole. Indeed, this statement has been verified by comparing the external admittance characteristics of a slot which was computed using the developed software with the impedance characteristics of a center-fed dipole found in the literature.

As the next step, using a single basis function, the admittance characteristics of a single isolated slot have been obtained and the results have been judged against the Stegen's experimental data. It is seen that with a single basis function, although the results are not exactly the same as the experimental data, a fair agreement can be achieved. There are several reasons behind this discrepancy. For instance, the wall thickness of the waveguide and the rounded edge slots are some of the reasons why the theoretical results do not match the experimental ones. Another factor is that the analysis has been carried out using a single basis function. In fact, if one increases the number of basis functions, s/he would expect to obtain better results. However, in this study most probably due to some mistakes in the developed code, the desired result could not be achieved when the number of basis functions was increased.

CHAPTER 4

CONCLUSION

In this study, the aim was to develop the core software of a MoM based solver which is to be a building block for a versatile software capable of solving an array of slots cut on a waveguide. A single slot on a waveguide is analyzed by using the developed code and the self admittance of the slot is calculated for different slot offset and length values. The results are compared with the experimental results found in the literature and a fair agreement is observed.

The integral equations required for the MoM solution have been presented in the second chapter. MATLAB has been used to calculate the internal and external scattering admittance entries of the MoM matrix. Because of its accuracy and speed, Gaussian quadrature has been preferred whenever numerical integration was needed. The major difficulty is encountered in the internal scattering self term computation. As described in Chapter 2, the infinite mode series in the internal scattering Green's function inherently does not converge because of the second order derivative; therefore, one needs to transfer this derivative to the basis and testing functions to obtain a convergent summation. The convergence problem of the internal Green's function is due to the fact that a singularity in the spatial domain results in a slowly convergent behavior in the spectral domain and the summation over the waveguide modes is a spectral domain summation.

In the third chapter the numerical results obtained from the MoM solution of a slot cut on the broad wall of a waveguide have been presented. Firstly, the external scattering equations obtained in Chapter 2 have been implemented in MATLAB.

Since a slot cut on an infinite ground plane and a center-fed dipole are dual structures, the external mutual and self admittance characteristics of a slot should resemble to the mutual and self impedance characteristics of a dipole. Indeed, this has been verified by comparing the external admittance characteristics of a slot which was computed using the developed software with the impedance characteristics of a center-fed dipole found in the literature. Afterwards, using a single basis function, the admittance characteristics of a single isolated slot have been computed and the results have been compared with the Stegen's experimental data. Although the results are not exactly the same as the experimental data, it is seen that with a single basis function, a fair agreement can be achieved. Because the developed software does not account for the wall thickness and the rounded edges, it is natural to have a difference between the Stegen's experimental data and the results obtained using the software. Another source of error is that the analysis has been carried out using a single basis function. In fact, if one increases the number of basis functions, s/he would obtain better results decreasing the error. To improve the accuracy the number of basis functions is increased; however reliable results could not be obtained most probably due to some mistakes in the developed code. Therefore as a first future work, the developed code will be improved to obtain reliable results with increased number of basis functions. Then the developed code will be used to analyze an array of slots instead of a single slot.

As another future work, the convergence problem encountered in the internal scattering in Chapter 2 should be further investigated. Instead of moving the derivatives onto the basis and testing functions, one can transform the internal scattering Green's function, which is indeed a spectral series, into a spatial series. Then the spatial series will be in a similar form like the free space Green's function, hence the methods which are used to calculate the external scattering Green's function can be utilized to evaluate the internal scattering. After resolving this convergence issue, one can generalize the single slot solution to the slot array case and compare the electric field results with the ones obtained from HFSS.

REFERENCES

[1] C. B. Top, (2006). "Design Of A Slotted Waveguide Array Antenna and Its Feed System", M.Sc. Dissertation, METU, Turkey; Sep 2006.

[2] H. G. Booker, “Slot Aerials and Their Relations to Complementary Wire Aerials (Babinet’s Principle)” JIEE(London), 93, pt.III A:pp. 620-626, 1946.

[3] W. H. Watson,The Physical Principles of Waveguide Transmission Antenna Systems, Clarendon Press, Oxford, 1947.

[4] A. F. Stevenson, “Theory of Slots in Rectangular Waveguides”, Journal of Applied Physics, vol. 19, pp.24-38, 1948.

[5] R. J. Stegen, ”Longitudinal Shunt Slot Characteristics” Technical Report 261, Hughes Technical Memorandum, Nov. 1971.(Stegen’s data are reproduced in R. C. Johnsson and H. Jasik, Antenna Engineering Handbook, McGraw Hill, New York,1984).

[6] R. S. Elliott, “On the Design of Traveling-Wave-Fed Longitudinal Shunt Slot Arrays” IEEE Trans. Antennas Propagation, vol. AP-27, no. 5, pp. 717-720, Sept. 1979.

[7] www.ansys.com (Last accessed on 23.03.2014)

[8] www.mig-germany.com (Last accessed on 23.03.2014)

[9] www.mathworks.com (Last accessed on 24.03.2014)

[10] R. S. Elliott and G. Stern, “Resonant Length of Longitudinal Slots and Validity of Circuit Representation: Theory and Experiment” IEEE Trans. Antennas Propagation, vol. AP-33, no.11, pp. 1264-1271, Nov. 1985.

[11] R. S. Elliott, “Antenna Theory and Design” Englewood Cliffs, NJ: Prentice Hall, 1981